ACS Energy LETTERS

http://pubs.acs.org/journal/aelccp

LETTER

Amorphous NiFe-OH/NiFeP Electrocatalyst Fabricated at Low Temperature for Water Oxidation Applications

Hanfeng Liang,[†] Appala N. Gandi,[†] Chuan Xia,[†] Mohamed N. Hedhili,[‡] Dalaver H. Anjum,[‡] Udo Schwingenschlögl,[†] and Husam N. Alshareef*[,†]

[†]Materials Science and Engineering and [‡]Imaging and Characterization Core Lab, King Abdullah University of Science and Technology (KAUST), Thuwal 23955-6900, Saudi Arabia

Supporting Information

ABSTRACT: Water splitting driven by electricity or sunlight is one of the most promising ways to address the global terawatt energy needs of future societies; however, its large-scale application is limited by the sluggish kinetics of the oxygen evolution reaction (OER). NiFe-based compounds, mainly oxides and hydroxides, are well-known OER catalysts and have been intensively studied; however, the utilization of the synergistic effect between two different NiFe-based materials to further boost the OER performance has not been achieved to date. Here, we report the rapid conversion of NiFe double hydroxide into metallic NiFeP using PH_3 plasma treatment and further construction of amorphous NiFe hydroxide/NiFeP/Ni foam as efficient and stable oxygen-evolving anodes. The strong electronic interactions between NiFe hydroxide and NiFeP significantly lower the adsorption energy of H_2O on the hybrid and thus lead to enhanced OER performance. As a result, the hybrid catalyst can deliver a geometrical current density of 300 mA cm^{-2} at an extremely low overpotential (258 mV, after ohmic-drop correction), along with a small Tafel slope of 39 mV $decade^{-1}$ and outstanding long-term durability in alkaline media.

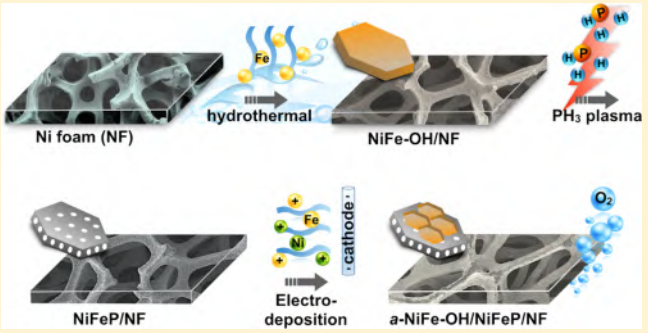

Water splitting ($H_2O \rightarrow H_2 + 1/2O_2$), ideally driven by solar power, is one of the most efficient and sustainable ways to produce molecular hydrogen (H_2) at high purity. If successful, it has the potential to address the global terawatt energy needs of future societies at no environmental cost.[1,2] Water oxidation ($2H_2O \rightarrow O_2 + 4H^+ + 4e^-$, also known as oxygen evolution reaction, or OER), one half-reaction of water splitting, has long been the bottleneck because it involves a four proton-coupled electron-transfer process that requires very high redox potential.[3−5] The reaction kinetics of the OER are sluggish; therefore, a substantial overpotential is required even when facilitated by precious metal-containing catalysts such as RuO_2 and IrO_2, which are considered to be state-of-the-art.[3,4] Hence, enormous efforts have been devoted to lowering both the overpotential and the catalyst cost while improving the stability. First-row transition-metal compounds such as NiCo-based oxides (or hydroxides) and borates are cost-efficient alternatives, though their performance still needs further improvement.[6−17] Among them, NiFe-based catalysts (mainly oxides and hydroxides) have been known to be active for the OER since last century and have recently seen a renewed interest because of their potential for replacing noble metal catalysts.[18,19] NiFe layered double hydroxide (LDH), a representative material of this family, is nowadays regarded as one of the most active OER catalysts.[18] By exfoliation or hybridization, it can now even outperform IrO_2 under alkaline conditions.[20,21] Although tremendous efforts have been directed toward enhancing the performance of NiFe oxides and (oxy)hydroxides, other earth-abundant NiFe-based catalysts such as phosphides have rarely been investigated despite the fact that they could also have the possibility to catalyze the OER.[22] Compared with oxides and hydroxides, most of which are either semiconducting or insulating, metal phosphides are highly conductive and consequently often show superior catalytic activities.[23,24] For example, Ni_2P and FeP are capable of catalyzing the OER at relatively low overpotentials (290 and 288 mV at 10 mA cm^{-2}, respectively).[25,26] The performance of monometallic phosphides may be further boosted through incorporation of extrinsic metals by utilizing the synergistic effect, though very little work has been conducted for this purpose to date.[6,27,28] In

Received: March 7, 2017
Accepted: April 11, 2017
Published: April 11, 2017

DOI: 10.1021/acsenergylett.7b00206
ACS Energy Lett. 2017, 2, 1035−1042

principle, thermal phosphorization of double hydroxides could form bimetallic phosphides; however, this remains to be explored.

Herein, we report the conversion of NiFe double hydroxide (NiFe-DH) into porous NiFeP through a recently developed PH_3 plasma treatment by our group at low temperature.[6] Commonly practiced chemical methods for the preparation of phosphides require high temperature (300−700 °C), long reaction time (several hours), and sometimes involve the use of organic solvents.[23,24] However, the plasma-assisted method enables rapid (∼15 min) synthesis of phosphides at low temperature (∼200 °C). The obtained porous NiFeP supported on Ni foam shows superior electrocatalytic activity toward water oxidation. Apart from searching for new low-cost, highly active, and robust catalysts, delicately nanostructuring the existing catalysts also provides an efficient way to improve the catalytic performance.[29] Ideally, a nanocatalyst should have a large surface area and high density of active sites. Furthermore, hybrid catalysts have also shown enhanced catalytic performance because of the strong coupling and synergistic effects between individual components.[30−32] Even though people are aware that the NiFe-based compounds are good OER catalysts, the utilization of the synergistic effect between two different NiFe-based materials to further boost the OER performance has not been achieved yet. We hence set out to design and construct a hierarchical electrocatalyst by electrodepositing an amorphous NiFe hydroxide layer onto porous NiFeP surface to further boost its performance. Such amorphous NiFe hydroxide/NiFeP/Ni foam (*a*-NiFe-OH/NiFeP/NF) hierarchical structure represents a prime example of hybrid electrocatalysts with multilevel nanostructures and has many advantages: (i) The metallic NiFeP greatly facilitates the electron transfer, lowering the charge-transfer resistance. (ii) The strong electronic interactions between the NiFeP and NiFe-OH would greatly improve the electrocatalytic activity. (iii) The porous structure exposes more active sites and enables close contact with electrolyte, thus promoting the ion diffusion. (iv) The amorphous NiFe hydroxide layer also contributes to the overall performance. In fact, amorphous materials are found to be even more active than their crystalline forms.[33−35] (v) The hierarchical structure helps the rapid release of oxygen gas bubbles under high current. (vi) Ni foam with open structure and high surface area serves as an ideal support for water oxidation catalysts and also contributes to the OER performance to some degree. As a result, the hierarchical nanoelectrodes achieved a geometrical current density of 300 mA cm^{-2} at an extremely low overpotential (258 mV) in alkaline media. Together with the small Tafel slope (39 mV dec^{-1}) and the good durability, the *a*-NiFe-OH/NiFeP/NF represents a promising cost-efficient, high-performance alternative for OER.

The preparation process of *a*-NiFe-OH/NiFeP hybrid catalyst supported on Ni foam is illustrated in Figure 1 (see Methods in the Supporting Information for details). Ni foam (Figure 1a) was used as a support for nanostructure growth and also served as current collector for water oxidation catalysis. The NiFe-DH precursor was first synthesized by hydrothermally reacting $Fe(NO_3)_3{\cdot}9H_2O$ and Ni foam with urea (Figure 1b). The resulting NiFe-OH nanoplates were then converted into porous NiFeP nanoplates using a recently developed PH_3 plasma-assisted process by our group (Figure 1c) at a relatively low temperature of 200 °C for 20 min. After PH_3 treatment, the Ni foam turned from yellow to black,

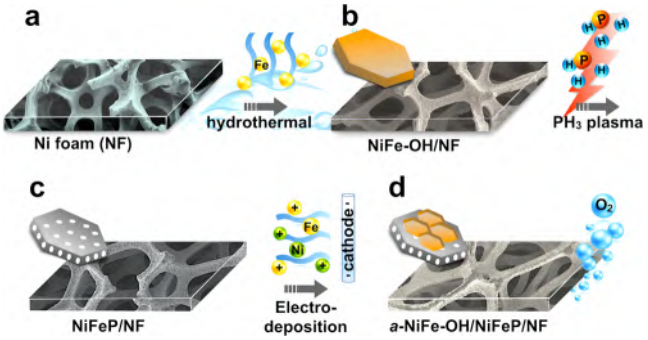

Figure 1. Scheme for the synthesis of *a*-NiFe-OH/NiFeP/NF hierarchical electrocatalyst for water oxidation: (a) Ni foam substrate, (b) NiFe-DH nanoplates grown on Ni foam via hydrothermal reaction, (c) conversion of NiFe-DH to porous NiFeP nanoplates using PH_3 plasma, and (d) electrodeposition of amorphous NiFe-OH nanosheet layer onto NiFeP and its application in electrocatalytic oxygen production.

indicating the formation of phosphides. Finally, an amorphous NiFe hydroxide nanosheet layer was electrodeposited onto the top of the NiFeP, leading to the formation of the hierarchical three-dimensaional (3D) *a*-NiFe-OH/NiFeP/NF electrocatalyst.

We first carried out X-ray diffraction (XRD) measurements to identify the phase of the products. As shown in Figure 2a, the diffraction peaks of the NiFe-DH precursor can be indexed to NiFe layered double hydroxide along with a minor $Fe(OH)_3$ phase, which should be caused by the favorable and fast hydrolysis of Fe^{3+} ions ($K_{sp}[Fe(OH)_3] = 4 \times 10^{-38}$).[36] The energy dispersive X-ray spectroscopy (EDS) analysis reveals that the ratio of Ni:Fe in the hexagonal NiFe-DH is 1.03:1 (Figure S1). After phosphidation, the diffraction pattern of the converted product is nearly identical to that of Ni_2P and Fe_2P, and the main peaks are found to be located between them, suggesting the formation of Ni_xFe_yP. The molar ratio of the Ni:Fe:P was determined to be 1.11:1:1.05 based on EDS result, giving a stoichiometric formula of $Ni_{1.11}FeP_{1.05}$ (Figure S2). This result demonstrates the efficacy of rapid low-temperature production of phosphides by PH_3 plasma. After further deposition of NiFe-OH, the diffraction peaks are almost the same as those of NiFeP/NF, indicating the amorphous nature of the topmost NiFe-OH layer. The morphology of the products was then revealed by scanning electron microscopy (SEM) and transmission electron microscopy (TEM). As shown in Figure 2b,c, the hydrothermally synthesized NiFe-DH is composed of vertically aligned nanoplates, which are commonly observed for hydroxides. Such platelike structures with a large surface area maximize the exposure of the surface active site.[37] The overall morphology is well-preserved after PH_3 plasma treatment. The as-converted NiFeP exhibits a hierarchical structure with thin nanoplates that are interconnected with each other, forming a highly open 3D network (Figure 2d), which could possibly offer high electrode−electrolyte interface area and good mechanical strength.[38] The TEM image (Figure 2e) shows that the individual nanoplates are continuous with smooth surface. Careful observation reveals that the nanoplates consist of many small crystalline nanoparticles (Figure S2), possibly formed because of the large strain caused by the crystal mismatch after phase conversion. The reorganization and aggregation of these nanoparticles result in the formation of pores, which would

DOI: 10.1021/acsenergylett.7b00206
ACS Energy Lett. 2017, 2, 1035−1042

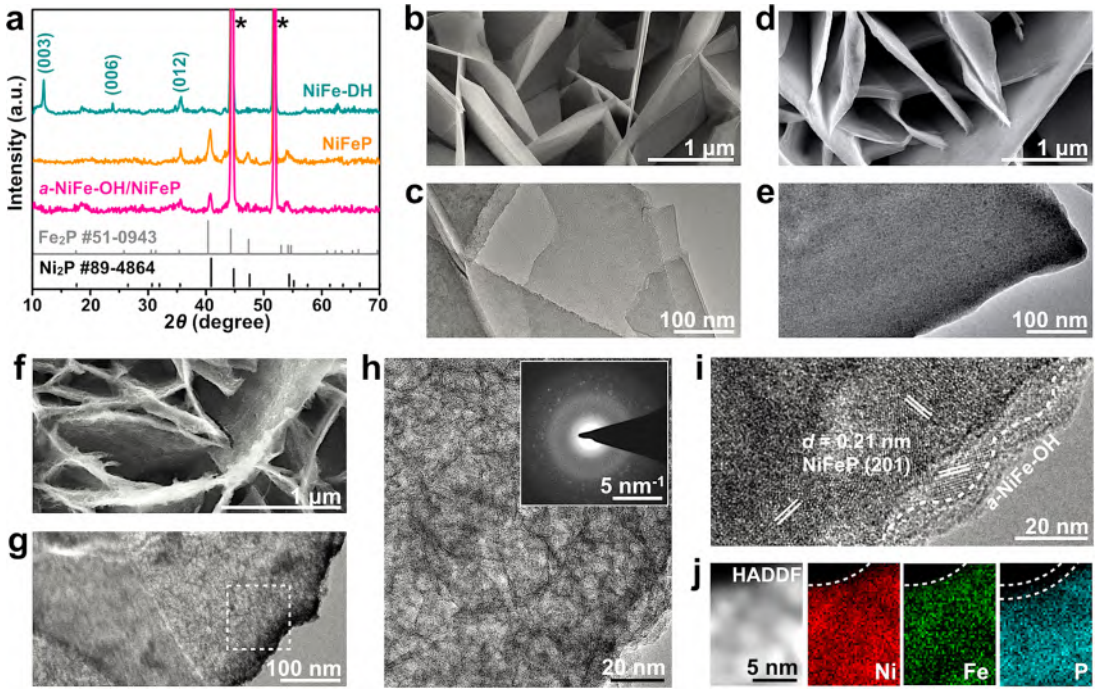

Figure 2. Structural characterization of NiFe-DH, NiFeP, and *a*-NiFe-OH/NiFeP on Ni foam. (a) XRD patterns of three NiFe-based electrocatalysts. The asterisks mark the diffraction peaks from Ni foam substrate. (b, c) SEM and TEM images of NiFe-DH nanoplates. (d, e) SEM and TEM images of NiFeP nanoplates. (f, g) SEM and TEM images of *a*-NiFe-OH/NiFeP hierarchical nanostructures. (h) TEM image and SAED pattern (inset) of *a*-NiFe-OH/NiFeP in the rectangle marked in panel g. (i) HRTEM image of NiFeP/NiFe-OH. (j) HADDF image of *a*-NiFe-OH/NiFeP and the corresponding EELS elemental maps showing the distribution of Ni, Fe, and P.

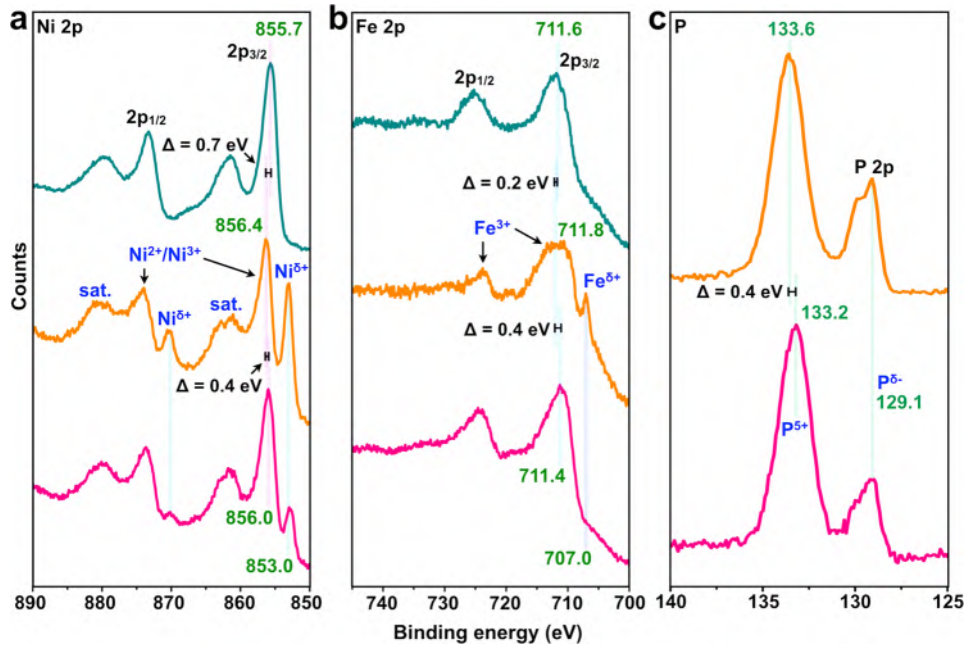

Figure 3. XPS characterization of NiFe-DH, NiFeP, and *a*-NiFe-OH/NiFeP on Ni foam: (a) Ni 2p, (b) Fe 2p, and (c) P 2p core-level spectra. Top to bottom in panels a and b: NiFe-DH, NiFeP, *a*-NiFe-OH/NiFeP; in panel c, NiFeP and *a*-NiFe-OH/NiFeP.

enable more active edge sites to be exposed and would thus promote electrocatalytic activity.[37] The scanning TEM-electron energy loss spectroscopy (STEM-EELS) elemental mapping shows the uniform distribution of Ni, Fe, and P (Figure S2), thus confirming the formation of NiFeP. After electrodeposition of NiFe-OH, a thin fluffy layer is observed on the initially smooth surface of the NiFeP nanoplates (Figure 2f). TEM investigation further reveals that the NiFeP nanoplates are uniformly coated by a thin nanosheet layer (Figure 2g,h and Figure S3). In addition, the selected area electron diffraction (SAED) pattern shows spots representative of the crystalline NiFeP and diffuse rings for the amorphous NiFe-OH layer (inset of Figure 2h), in agreement with the XRD result. Figure 2i displays a typical high-resolution TEM (HRTEM) image, wherein a crystalline−amorphous interface can be clearly seen (as indicated by a white dashed line), suggesting a thin NiFe-

DOI: 10.1021/acsenergylett.7b00206
ACS Energy Lett. 2017, 2, 1035−1042

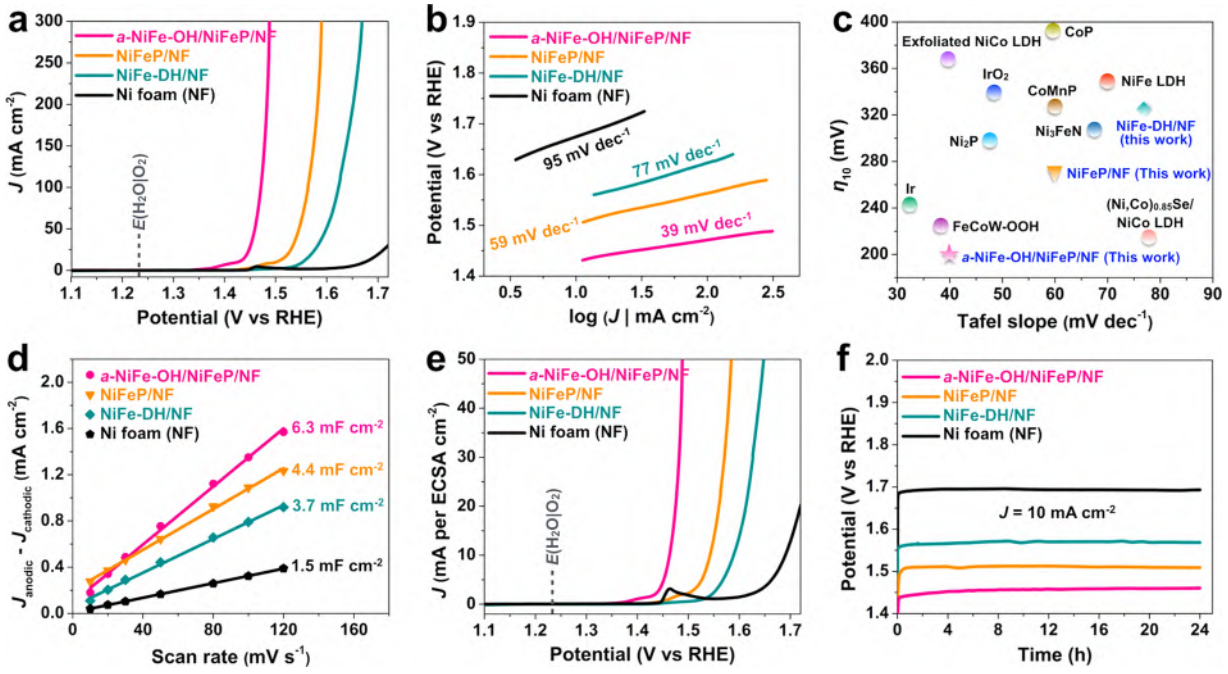

Figure 4. Electrocatalytic water oxidation over the NiFe-OH/NF, NiFeP/NF, and *a*-NiFe-OH/NiFeP/NF catalysts in 1 M KOH. (a) *IR*-corrected polarization curves for the NiFeP/NiFe-OH recorded at a scan rate of 0.5 mV s^{-1}, along with NiFeP, NiFe-OH, and Ni foam for comparison. (b) Polarization curves-derived Tafel slopes for the corresponding electrocatalysts. (c) Overpotential required at 10 mA cm^{-2} (η_{10}) and Tafel slope comparison of the catalysts in this work with other recently reported high-performance OER electrocatalysts. (d) Plots showing the extraction of the double-layer capacitances allow the estimation of the electrochemically active surface area (ECSA). (e) ECSA-normalized polarization curves. (f) Long-term stability test carried out at a constant current density of 10 mA cm^{-2}. References cited in panel c: exfoliated NiCo LDH,[7] NiFe LDH,[20] CoP,[57] Ni_2P,[25] CoMnP,[27] Ni_3FeN,[58] $(Ni,Co)_{0.85}Se$/NiCo LDH,[59] FeCoW-OOH,[60] IrO_2,[20] and Ir.[61]

OH layer on the surface of the NiFeP. The interplanar spacing was determined to be 0.21 nm, corresponding to the (201) planes of NiFeP. To further identify the core−shell structure, we carried out the STEM-EELS elemental mapping. As shown in Figure 2j, the Ni and Fe are homogeneously distributed throughout the whole nanoplates, whereas the P presents a surface deficient layer, which confirms that the NiFeP is indeed uniformly coated by amorphous NiFe-OH.

X-ray photoelectron spectroscopy (XPS) measurements were further performed to probe the chemical valence states as well as to investigate the surface change after phosphidation. Figure 3 shows the Ni 2p, Fe 2p, and P 2p core-level XPS spectra. The Ni $2p_{3/2}$ (Figure 3a) region for the NiFe-DH precursor shows two main peaks at 855.7 and 861.2 eV that can be ascribed to the oxidized Ni^{2+}/Ni^{3+} in $Ni(OH)_2$/NiOOH and the corresponding satellite peak, respectively.[39,40] After plasma phosphidation, the peak centered at 855.7 eV shifts to a higher energy (~0.7 eV), indicating a change in the electronic structure occurs upon the phase conversion. This peak at 856.4 eV is possibly related to the Ni^{2+} ions in the phosphate as a consequence of surface oxidation of phosphide.[40] Furthermore, a new Ni $2p_{3/2}$ peak located at 853.0 eV is observed, which could be ascribed to the Ni−P bonding.[41] The binding energy is close to that of metallic Ni (852.6 eV),[42] suggesting the presence of partially charged Ni species ($Ni^{\delta+}$, δ is likely close to 0). For Fe 2p (Figure 3b), the Fe $2p_{3/2}$ and Fe $2p_{1/2}$ peaks are located at 711.6 and 725.5 eV, respectively, which are the characteristic binding energies of Fe^{3+} in FeOOH.[39,43] After phosphidation, a new Fe $2p_{3/2}$ peak appears at the binding energy of 707.0 eV, which can be ascribed to the Fe−P bonding, in good agreement with previous reports.[44−46] This binding energy is also close to that of Fe^0 (706.8 eV),[47] indicating that the Fe in Fe−P carries a partially positive charge ($Fe^{\delta+}$). As for the P 2p region (Figure 3c), the main peak located at 129.1 eV is assigned to reduced phosphorus ($P^{\delta-}$) in the form of phosphides.[46,48] The peak at 133.6 eV can be attributed to the oxidized phosphorus in phosphate (P_2O_5 or PO_4^{3-}), indicating the surface is oxidized, which is commonly seen in metal phosphides under air exposure.[49,50] The above XPS result demonstrates the successful conversion of NiFe-DH into NiFeP via the low-temperature PH_3 plasma phosphidation process. The XPS spectra for the *a*-NiFe-OH/NiFeP show that the intensity of the peaks associated with $Ni^{\delta+}$, $Fe^{\delta+}$, and $P^{\delta-}$ species is weakened compared to that of NiFeP, which is due to the deposited NiFe-OH layer that attenuates the XPS signal collected from the NiFeP sublayer. In addition, the Ni 2p and Fe 2p peaks both shift to lower binding energies (~0.4 eV). This negative shift is attributed mostly to the Ni and Fe species in the deposited *a*-NiFe-OH layer and to the strong electronic interactions between NiFeP and NiFe-OH, where the protons are transferred from positively charged Ni and Fe in *a*-NiFe-OH to the P species in NiFeP. Such strong electronic interactions could possibly improve the electrocatalytic activity of the *a*-NiFe-OH/NiFeP, as demonstrated for other hybrid systems.[30−32]

We then accessed the electrocatalytic activity of the *a*-NiFe-OH/NiFeP/NF toward the OER in 1 M KOH (pH = 13.6) using a standard three-electrode system (see Methods for details). Figure 4a shows the *IR* (*I*, current; *R*, resistance)-corrected polarization curves of the *a*-NiFe-OH/NiFeP/NF electrode along with NiFeP/NF and NiFe-DH/NF for comparison (see the raw data and the Nyquist plots in Figure S4). The NiFe-DH exhibits good activity with an overpotential of 323 mV at 10 mA cm^{-2}, consistent with that previously

DOI: 10.1021/acsenergylett.7b00206
ACS Energy Lett. 2017, 2, 1035−1042

reported for NiFe-based (oxy)hydroxides in alkaline solution.[20] After conversion into NiFeP, the OER performance greatly improved, which is possibly due to the porous structures as revealed by microscopy and the metallic nature of the NiFeP that facilitates the electron transfer (Figure S5). As a result, the NiFeP/NF requires only 270 mV to achieve the current density of 10 mA cm^{-2}, which is 53 and 170 mV less than that of NiFe-DH/NF and pure Ni foam, respectively. This overpotential compares favorably to those recently reported for metal phosphides and the most active non-noble metal OER catalysts.[25−27,51−55] For example, we also synthesized Ni_2P nanoplates on Ni foam (Figure S6) and further compared their OER performance. The result shows that the NiFeP/NF is much more active than Ni_2P/NF (Figure S7), which confirms the efficacy of our strategy of incorporating Fe into Ni_2P to enhance the OER performance. This result implies that the extrinsic metal substitution may serve as a general strategy for enhancing the performance of monometallic phosphides in electrocatalysis and many other applications. Of note, the NiFeP/NF even surpasses the IrO_2 and RuO_2 (Figure S8a), which are considered as the state-of-the-art OER catalysts. The performance is further significantly boosted after NiFe-OH coating. The *a*-NiFe-OH/NiFeP/NF only needs an overpotential as low as 199 mV at 10 mA cm^{-2} and can achieve a large current density of 300 mA cm^{-2} at an extremely low overpotential of 258 mV, which is practically valuable for the rapid electrocatalytic water splitting. In sharp contrast, the current densities are only 8.6 and 1.9 mA cm^{-2} at 258 mV for NiFeP and NiFe-DH, respectively. Note that the Ni foam support shows negligible activity below 1.6 V vs RHE, further supporting the conclusion that the high performance of *a*-NiFe-OH/NiFeP/NF mainly comes from the *a*-NiFe-OH/NiFeP. The superior OER performance is further revealed by the Tafel slopes (Figure 4b), which represent the inherent properties of the catalysts. The *a*-NiFe-OH/NiFeP/NF possesses a Tafel slope of 39 mV dec^{-1}, which is much smaller than that of NiFeP (59 mV dec^{-1}), NiFe-DH (77 mV dec^{-1}), and Ni foam (95 mV dec^{-1}). It is worth mentioning that the metallic NiFeP is an indispensable part of the hybrid electrocatalyst for the high OER performance. We have prepared two control catalysts, namely *a*-NiFe-OH/NF and *a*-NiFe-OH/NiFe-DH/NF (see SEM images in Figure S9), and further compared their OER performance with the *a*-NiFe-OH/NiFeP/NF. The result shows that the *a*-NiFe-OH/NiFeP/NF exhibits a much higher activity than that of *a*-NiFe-OH/NF and *a*-NiFe-OH/NiFe-DH/NF (Figure S10), which may result from the metallic feature of NiFeP that favors the electron transfer. The effect of Ni/Fe ratio in the deposited *a*-NiFe-OH layer on the OER performance was also investigated, and the result reveals that the *a*-NiFe-OH/NiFeP/NF with initial Ni/Fe ratio of 1:1 exhibits the optimal performance (Figure S11). These results establish our *a*-NiFe-OH/NiFeP/NF as an earth-abundant and efficient OER catalyst that is superior to most, if not all, recently reported high-performance electrocatalysts, including Ir and IrO_2 (Figure 4c and also see the comparison in Table S1).[53−55] To elucidate the origin of the disparity in the OER performance among different catalysts, we conducted the Brunauer−Emmett−Teller (BET) surface area measurements (Figure S12), and the result shows that the *a*-NiFe-OH/NiFeP/NF has the largest specific surface area of 22.5 $m^2 g^{-1}$, followed by NiFeP/NF (11.3 $m^2 g^{-1}$), and then NiFe-DH/NF (7.6 $m^2 g^{-1}$). It is worth mentioning that the Ni foam has a small contribution to the surface area but has a significant contribution to the total mass (the mass loadings of the three NiFe materials are 1.6−2.1 mg cm^{-2}, compared to 72 mg cm^{-2} of Ni foam), which could lower the real surface area of the three NiFe catalysts. In view of this, the electrochemically active surface area (ECSA) would be a more reliable metric for comparison. We therefore carried out a simple cyclic voltammetry (CV) measurement to determine the double-layer capacitance (C_{dl}), which is linearly proportional to the electrochemically active surface area (ECSA), thus serving as an estimate of the ECSA of the solid−liquid interface.[56] Figure 4d shows the plots of difference in current ($\Delta j = j_a - j_c$ at 0.95 V vs RHE) against the scan rate (see CV results in Figure S13). The *a*-NiFe-OH/NiFeP/NF possesses the highest C_{dl} of 6.3 mF cm^{-2}, which is nearly 1.5 and 2 times that of the NiFeP (4.4 mF cm^{-2}) and NiFe-DH (3.6 mF cm^{-2}), respectively, indicating more exposure of the active sites in the *a*-NiFe-OH/NiFeP/NF. However, it is unlikely that such a small variation in ECSA fully accounts for the dramatic difference in performance. Indeed, when we normalized the current density to ECSA, the *a*-NiFe-OH/NiFeP/NF still shows current densities that are much larger than those of the other two catalysts at the same overpotentials (Figure 4e), indicating that the hybrid *a*-NiFe-OH/NiFeP/NF is intrinsically more active than NiFeP/NF and NiFe-DH/NF individuals. We further calculated the mass activity and the turnover frequency (TOF) using these data. The *a*-NiFe-OH/NiFeP/NF achieved a mass activity of ∼93.3 A g^{-1} at a low overpotential of 250 mV (Figure S8b), which is equivalent to a TOF of ∼0.036 s^{-1}. This value is much higher than that of NiFe-DH, NiFeP, and even IrO_2/RuO_2 (see the comparison in Table S2), supporting the high intrinsic activity of the *a*-NiFe-OH/NiFeP/NF.

Aside from the high catalytic activity, the operating stability is also essential to practical application. We conducted the stability test by applying a constant current density of 10 mA cm^{-2} continuously for 24 h. As shown in Figure 4f, no appreciable deactivation is observed for the three NiFe-based electrocatalysts in this time interval. To further assess possible morphological or structural changes after electrocatalysis, we carried out XRD characterization on the post-OER electrodes. The results show that the NiFe-DH is converted into NiFe oxide, while the NiFeP and *a*-NiFeP-OH/NiFeP remained unchanged in the bulk phase (Figure S14a). The phase evolution in NiFe-DH results in significant morphological change. As observed by SEM, the NiFe-DH nanoplates completely decompose into nanoparticles (Figure S14b). In contrast, the NiFeP (Figure S14c) and *a*-NiFeP-OH/NiFeP (Figure S14d) preserve the overall plate-like morphology. Careful observation reveals that the surface generally becomes much rougher and is coated by a thin particulate layer, which may prevent the nanoplates from further breakdown under severe oxygen bubble evolution. It has been reported that the real OER active sites for phosphides are the surface oxides (or oxyhydroxides) that in situ formed during the electrocatalysis.[6,52,62] In an effort to understand the composition of the surface layer, we further performed the XPS analysis (Figure S15). For both the NiFeP and *a*-NiFe-OH/NiFeP, the low-valent Ni ($Ni^{\delta+}$), Fe ($Fe^{\delta+}$), and P ($P^{\delta-}$) peaks that originally located at 853.0, 707.0, and 129.1 eV, respectively, in the freshly synthesized samples (Figure 3) disappear, suggesting a surface oxidation of the materials into metal oxide species. Note that the P^{5+} species are still detectable; however, they would eventually be oxidized into oxyhydroxides, as demonstrated by a previous study[63] and confirmed by the XPS analysis

DOI: 10.1021/acsenergylett.7b00206
ACS Energy Lett. 2017, 2, 1035−1042

on our post OER samples after prolonged operation time (Figure S16). This observation is in accordance with a recent report in which Ni_2P was oxidized into NiO_x under the oxidative conditions of OER.[25] The surface oxide species were further identified by HRTEM. We observed two sets of the lattice spacings that can be assigned to NiFeP and Ni_xFe_yO for the *a*-NiFe-OH/NiFeP after the OER (Figure S17). We noted that the post-OER Ni 2p and Fe 2p XPS spectra for all the three electrocatalysts have the same shape and show no significant shift in binding energy (Figure S15), which means after the OER, the surfaces of all three samples are oxidized to NiFe oxyhydroxides, which is supposed to be the real active sites. Because the surface chemistry changes, we therefore further monitored the leaching rate of P for *a*-NiFe-OH/NiFeP during the long-term stability test, and the result shows that the leaching rate of P is quite slow. The concentration of P in electrolyte after 24 h OER catalysis is only 1.01 ppm as determined by ICP (Figure S18).

It might be then confusing that the three electrocatalysts show significantly different apparent OER performance even though their real active sites for OER are essentially the same, namely, NiFe oxyhydroxides. It is also interesting to note that a recent study has shown that the $Ni_xFe_{1-x}Se_2$-derived oxides exhibit higher OER activity than $Ni_xFe_{1-x}O$ though the origin of the high activity is not yet clear.[64] Even for the well-known NiFe oxyhydroxides, which have been emerged as the most active OER electrocatalysts and have been widely studied in recent years, the origin of the synergy between Ni and Fe in these materials is still not fully understood.[39,65] Therefore, here we will discuss only some of the possibilities that could lead to the high OER performance of the *a*-NiFe-OH/NiFeP/NF. We believe that the hierarchical structure plays an important role, which enables the close contact with electrolyte; promotes the ion diffusion; and more importantly, results in higher number of active sites, as confirmed by the ECSA analysis shown in Figure 4d. The unique core−shell structure also facilitates the electron transfer from the inner metallic NiFeP to the outer shell *a*-NiFe-OH layer. Note that the *a*-NiFe-OH/NiFeP/NF possesses the lowest charge-transfer resistance among the three samples (Figure S4b). This favorable electron transfer would improve the catalytic activity. Furthermore, it has been demonstrated that the amorphous materials generally exhibit catalytic activity superior to that of comparable crystalline materials.[33−35] Amorphous materials have a larger amount of randomly oriented bonds and thus a greater density of surface unsaturated sites than crystalline materials, which enhance the adsorption of reactants and therefore result in higher activity.[66] Moreover, the relaxation energy of the structural distortion has been shown to be strongly related with the activation energy of the surface reaction.[67] Amorphous materials have higher structural flexibility compared with crystalline materials and thus generally result in superior catalytic activity.[35] To confirm the superior activity of the *a*-NiFe-OH/NF, we have prepared crystalline NiFe-OH/NF (*c*-NiFe-OH/NF) by annealing *a*-NiFe-OH in Ar at 200 °C for 2 h and then investigated the OER performance for comparison. The result indeed shows that the *a*-NiFe-OH/NF exhibits activity that is higher than that of *c*-NiFe-OH/NF in terms of both the lower overpotentials and the smaller Tafel slope (Figure S19). Aside from these exciting features resulting from the unique hierarchical nanostructures, our XPS result suggests that there are strong electronic interactions between NiFeP and *a*-NiFe-OH. We noted that it has been previously demonstrated that such strong electronic interactions between two individual components in the hybrid electrocatalysts could effectively alter the electronic structure and lower the free energy for adsorption of intermediates, therefore leading to an enhanced catalytic activity.[30−32] We thus calculated the adsorption energy for H_2O on NiFe-OH, NiFeP, and NiFe-OH/NiFeP (see structure models in Figure S20) to evaluate the effect of the strong electronic interactions on water splitting. The result shows that the adsorption energy for H_2O on NiFe-OH/NiFeP (−2.73 eV) is much lower than that on NiFe-OH (−0.38 eV) and NiFeP (−0.35 eV), suggesting that the H_2O adsorption is much more favorable (Figure S21). This behavior will also improve the electrocatalytic activity of *a*-NiFe-OH/NiFeP/NF.[58]

In summary, we have demonstrated the low-temperature rapid conversion of NiFe-DH into porous NiFeP nanoplates using plasma. The resultant metallic NiFeP already shows high catalytic activity toward the OER that is superior to most of the state-of-the-art OER electrocatalysts, while its performance can be further significantly boosted by constructing hierarchical amorphous NiFe-OH/NiFeP core−shell nanostructures on Ni foam. Specifically, the hybrid *a*-NiFe-OH/NiFeP/NF achieved stable performance in alkaline solution with an extremely low overpotential of 258 mV at a high current density of 300 mA cm^{-2} and a small Tafel slope of 39 mV dec^{-1}, making it one of the most active OER catalysts. The high activity is attributed to the unique architecture, the metallic nature of NiFeP, and the strong electronic interactions between *a*-NiFe-OH and NiFeP. Such rational design and construction of hierarchical nanostructures should be generally applicable for significantly enhancing the catalytic and many other applications of various transition-metal-based compounds.

■ ASSOCIATED CONTENT

Supporting Information

The Supporting Information is available free of charge on the ACS Publications website at DOI: 10.1021/acsenergylett.7b00206.

Experimental details, additional supporting data, and comparison of catalytic performance (PDF)

■ AUTHOR INFORMATION

Corresponding Author

*E-mail: husam.alshareef@kaust.edu.sa.

ORCID

Hanfeng Liang: 0000-0002-1778-3975
Udo Schwingenschlögl: 0000-0003-4179-7231
Husam N. Alshareef: 0000-0001-5029-2142

Notes

The authors declare no competing financial interest.

■ ACKNOWLEDGMENTS

Research reported in this publication was supported by funding from King Abdullah University of Science and Technology (KAUST).

■ REFERENCES

(1) Lewis, N. S.; Nocera, D. G. Powering the Planet: Chemical Challenges in Solar Energy Utilization. *Proc. Natl. Acad. Sci. U. S. A.* **2006**, *103*, 15729−15735.

(2) Nocera, D. G. The Artificial Leaf. *Acc. Chem. Res.* **2012**, *45*, 767−776.

DOI: 10.1021/acsenergylett.7b00206
ACS Energy Lett. 2017, 2, 1035−1042

(3) Jiao, Y.; Zheng, Y.; Jaroniec, M.; Qiao, S. Z. Design of Electrocatalysts for Oxygen-and Hydrogen-Involving Energy Conversion Reactions. *Chem. Soc. Rev.* **2015**, *44*, 2060−2086.
(4) Hong, W. T.; Risch, M.; Stoerzinger, K. A.; Grimaud, A.; Suntivich, J.; Shao-Horn, Y. Toward the Rational Design of Non-Precious Transition Metal Oxides for Oxygen Electrocatalysis. *Energy Environ. Sci.* **2015**, *8*, 1404−1427.
(5) Zhu, Y. P.; Guo, C.; Zheng, Y.; Qiao, S.-Z. Surface and Interface Engineering of Noble-Metal-Free Electrocatalysts for Efficient Energy Conversion Processes. *Acc. Chem. Res.* **2017**, DOI: 10.1021/acs.accounts.6b00635.
(6) Liang, H.; Gandi, A. N.; Anjum, D. H.; Wang, X.; Schwingenschlögl, U.; Alshareef, H. N. Plasma-Assisted Synthesis of NiCoP for Efficient Overall Water Splitting. *Nano Lett.* **2016**, *16*, 7718−7725.
(7) Liang, H.; Meng, F.; Cabán-Acevedo, M.; Li, L.; Forticaux, A.; Xiu, L.; Wang, Z.; Jin, S. Hydrothermal Continuous Flow Synthesis and Exfoliation of NiCo Layered Double Hydroxide Nanosheets for Enhanced Oxygen Evolution Catalysis. *Nano Lett.* **2015**, *15*, 1421−1427.
(8) Dincă, M.; Surendranath, Y.; Nocera, D. G. Nickel-Borate Oxygen-Evolving Catalyst That Functions under Benign Conditions. *Proc. Natl. Acad. Sci. U. S. A.* **2010**, *107*, 10337−10341.
(9) Esswein, A. J.; Surendranath, Y.; Reece, S. Y.; Nocera, D. G. Highly Active Cobalt Phosphate and Borate Based Oxygen Evolving Catalysts Operating in Neutral and Natural Waters. *Energy Environ. Sci.* **2011**, *4*, 499−504.
(10) Ming, F.; Liang, H.; Shi, H.; Xu, X.; Mei, G.; Wang, Z. MOF-Derived Co-Doped Nickel Selenide/C Electrocatalysts Supported on Ni Foam for Overall Water Splitting. *J. Mater. Chem. A* **2016**, *4*, 15148−15155.
(11) Lu, X. F.; Gu, L. F.; Wang, J. W.; Wu, J. X.; Liao, P. Q.; Li, G. R. Bimetal-Organic Framework Derived $CoFe_2O_4$/C Porous Hybrid Nanorod Arrays as High-Performance Electrocatalysts for Oxygen Evolution Reaction. *Adv. Mater.* **2017**, *29*, 1604437.
(12) Wang, A.-L.; Xu, H.; Li, G.-R. NiCoFe Layered Triple Hydroxides with Porous Structures as High-Performance Bifunctional Electrocatalysts for Overall Water Splitting. *ACS Energy Lett.* **2016**, *1*, 445−453.
(13) Duan, J.; Chen, S.; Vasileff, A.; Qiao, S. Z. Anion and Cation Modulation in Metal Compounds for Bifunctional Overall Water Splitting. *ACS Nano* **2016**, *10*, 8738−8745.
(14) Ling, T.; Yan, D.-Y.; Jiao, Y.; Wang, H.; Zheng, Y.; Zheng, X.; Mao, J.; Du, X.-W.; Hu, Z.; Jaroniec, M.; et al. Engineering Surface Atomic Structure of Single-Crystal Cobalt (II) Oxide Nanorods for Superior Electrocatalysis. *Nat. Commun.* **2016**, *7*, 12876.
(15) Meng, C.; Ling, T.; Ma, T. Y.; Wang, H.; Hu, Z.; Zhou, Y.; Mao, J.; Du, X. W.; Jaroniec, M.; Qiao, S. Z. Atomically and Electronically Coupled Pt and Coo Hybrid Nanocatalysts for Enhanced Electrocatalytic Performance. *Adv. Mater.* **2017**, *29*, 1604607.
(16) Zhu, Y. P.; Ma, T. Y.; Jaroniec, M.; Qiao, S. Z. Self-Templating Synthesis of Hollow Co_3O_4 Microtube Arrays for Highly Efficient Water Electrolysis. *Angew. Chem., Int. Ed.* **2017**, *56*, 1324−1328.
(17) Zheng, Y.; Jiao, Y.; Zhu, Y.; Cai, Q.; Vasileff, A.; Li, L. H.; Han, Y.; Chen, Y.; Qiao, S.-Z. Molecule-Level G-C_3N_4 Coordinated Transition Metals as a New Class of Electrocatalysts for Oxygen Electrode Reactions. *J. Am. Chem. Soc.* **2017**, *139*, 3336−3339.
(18) Gong, M.; Dai, H. A Mini Review of NiFe-Based Materials as Highly Active Oxygen Evolution Reaction Electrocatalysts. *Nano Res.* **2015**, *8*, 23−39.
(19) Gong, M.; Li, Y.; Wang, H.; Liang, Y.; Wu, J. Z.; Zhou, J.; Wang, J.; Regier, T.; Wei, F.; Dai, H. An Advanced Ni−Fe Layered Double Hydroxide Electrocatalyst for Water Oxidation. *J. Am. Chem. Soc.* **2013**, *135*, 8452−8455.
(20) Song, F.; Hu, X. Exfoliation of Layered Double Hydroxides for Enhanced Oxygen Evolution Catalysis. *Nat. Commun.* **2014**, *5*, 4477.
(21) Long, X.; Li, J.; Xiao, S.; Yan, K.; Wang, Z.; Chen, H.; Yang, S. A Strongly Coupled Graphene and FeNi Double Hydroxide Hybrid as an Excellent Electrocatalyst for the Oxygen Evolution Reaction. *Angew. Chem., Int. Ed.* **2014**, *53*, 7584−7588.
(22) Read, C. G.; Callejas, J. F.; Holder, C. F.; Schaak, R. E. General Strategy for the Synthesis of Transition Metal Phosphide Films for Electrocatalytic Hydrogen and Oxygen Evolution. *ACS Appl. Mater. Interfaces* **2016**, *8*, 12798−12803.
(23) Shi, Y.; Zhang, B. Recent Advances in Transition Metal Phosphide Nanomaterials: Synthesis and Applications in Hydrogen Evolution Reaction. *Chem. Soc. Rev.* **2016**, *45*, 1529−1541.
(24) Callejas, J. F.; Read, C. G.; Roske, C. W.; Lewis, N. S.; Schaak, R. E. Synthesis, Characterization, and Properties of Metal Phosphide Catalysts for the Hydrogen-Evolution Reaction. *Chem. Mater.* **2016**, *28*, 6017−6044.
(25) Stern, L.-A.; Feng, L.; Song, F.; Hu, X. Ni_2P as a Janus Catalyst for Water Splitting: The Oxygen Evolution Activity of Ni_2P Nanoparticles. *Energy Environ. Sci.* **2015**, *8*, 2347−2351.
(26) Yan, Y.; Xia, B. Y.; Ge, X.; Liu, Z.; Fisher, A.; Wang, X. A Flexible Electrode Based on Iron Phosphide Nanotubes for Overall Water Splitting. *Chem. - Eur. J.* **2015**, *21*, 18062−18067.
(27) Li, D.; Baydoun, H.; Verani, C. u. N.; Brock, S. L. Efficient Water Oxidation Using Comnp Nanoparticles. *J. Am. Chem. Soc.* **2016**, *138*, 4006−4009.
(28) Tan, Y.; Wang, H.; Liu, P.; Shen, Y.; Cheng, C.; Hirata, A.; Fujita, T.; Tang, Z.; Chen, M. Versatile Nanoporous Bimetallic Phosphides Towards Electrochemical Water Splitting. *Energy Environ. Sci.* **2016**, *9*, 2257.
(29) Faber, M. S.; Jin, S. Earth-Abundant Inorganic Electrocatalysts and Their Nanostructures for Energy Conversion Applications. *Energy Environ. Sci.* **2014**, *7*, 3519−3542.
(30) Feng, J. X.; Ding, L. X.; Ye, S. H.; He, X. J.; Xu, H.; Tong, Y. X.; Li, G. R. $Co(OH)_2$@PANI Hybrid Nanosheets with 3D Networks as High-Performance Electrocatalysts for Hydrogen Evolution Reaction. *Adv. Mater.* **2015**, *27*, 7051−7057.
(31) Feng, J. X.; Ye, S. H.; Xu, H.; Tong, Y. X.; Li, G. R. Design and Synthesis of FeOOH/CeO_2 Heterolayered Nanotube Electrocatalysts for the Oxygen Evolution Reaction. *Adv. Mater.* **2016**, *28*, 4698−4703.
(32) Feng, J. X.; Xu, H.; Dong, Y. T.; Ye, S. H.; Tong, Y. X.; Li, G. R. FeOOH/Co/FeOOH Hybrid Nanotube Arrays as High-Performance Electrocatalysts for the Oxygen Evolution Reaction. *Angew. Chem., Int. Ed.* **2016**, *55*, 3694−3698.
(33) Smith, R. D.; Prévot, M. S.; Fagan, R. D.; Zhang, Z.; Sedach, P. A.; Siu, M. K. J.; Trudel, S.; Berlinguette, C. P. Photochemical Route for Accessing Amorphous Metal Oxide Materials for Water Oxidation Catalysis. *Science* **2013**, *340*, 60−63.
(34) Indra, A.; Menezes, P. W.; Sahraie, N. R.; Bergmann, A.; Das, C.; Tallarida, M.; Schmeißer, D.; Strasser, P.; Driess, M. Unification of Catalytic Water Oxidation and Oxygen Reduction Reactions: Amorphous Beat Crystalline Cobalt Iron Oxides. *J. Am. Chem. Soc.* **2014**, *136*, 17530−17536.
(35) Tsuji, E.; Imanishi, A.; Fukui, K.-i.; Nakato, Y. Electrocatalytic Activity of Amorphous RuO_2 Electrode for Oxygen Evolution in an Aqueous Solution. *Electrochim. Acta* **2011**, *56*, 2009−2016.
(36) Meng, F.; Morin, S. A.; Jin, S. Rational Solution Growth of α-FeOOH Nanowires Driven by Screw Dislocations and Their Conversion to α-Fe_2O_3 Nanowires. *J. Am. Chem. Soc.* **2011**, *133*, 8408−8411.
(37) Liang, H.; Li, L.; Meng, F.; Dang, L.; Zhuo, J.; Forticaux, A.; Wang, Z.; Jin, S. Porous Two-Dimensional Nanosheets Converted from Layered Double Hydroxides and Their Applications in Electrocatalytic Water Splitting. *Chem. Mater.* **2015**, *27*, 5702−5711.
(38) Zhang, G.; Lou, X. W. D. General Solution Growth of Mesoporous $NiCo_2O_4$ Nanosheets on Various Conductive Substrates as High-Performance Electrodes for Supercapacitors. *Adv. Mater.* **2013**, *25*, 976−979.
(39) Friebel, D.; Louie, M. W.; Bajdich, M.; Sanwald, K. E.; Cai, Y.; Wise, A. M.; Cheng, M.-J.; Sokaras, D.; Weng, T.-C.; Alonso-Mori, R.; et al. Identification of Highly Active Fe Sites in (Ni, Fe)OOH for Electrocatalytic Water Splitting. *J. Am. Chem. Soc.* **2015**, *137*, 1305−1313.

DOI: 10.1021/acsenergylett.7b00206
ACS Energy Lett. 2017, 2, 1035−1042

(40) Infantes-Molina, A.; Cecilia, J.; Pawelec, B.; Fierro, J.; Rodríguez-Castellón, E.; Jiménez-López, A. Ni_2P and CoP Catalysts Prepared from Phosphite-Type Precursors for HDS−HDN Competitive Reactions. *Appl. Catal., A* **2010**, *390*, 253−263.
(41) Ledendecker, M.; Krick Calderón, S.; Papp, C.; Steinrück, H. P.; Antonietti, M.; Shalom, M. The Synthesis of Nanostructured Ni_5P_4 Films and Their Use as a Non-Noble Bifunctional Electrocatalyst for Full Water Splitting. *Angew. Chem., Int. Ed.* **2015**, *54*, 12361−12365.
(42) Grosvenor, A. P.; Biesinger, M. C.; Smart, R. S. C.; McIntyre, N. S. New Interpretations of XPS Spectra of Nickel Metal and Oxides. *Surf. Sci.* **2006**, *600*, 1771−1779.
(43) Harvey, D. T.; Linton, R. W. Chemical Characterization of Hydrous Ferric Oxides by X-Ray Photoelectron Spectroscopy. *Anal. Chem.* **1981**, *53*, 1684−1688.
(44) Masud, J.; Umapathi, S.; Ashokaan, N.; Nath, M. Iron Phosphide Nanoparticles as an Efficient Electrocatalyst for the OER in Alkaline Solution. *J. Mater. Chem. A* **2016**, *4*, 9750−9754.
(45) Huang, Z.; Lv, C.; Chen, Z.; Chen, Z.; Tian, F.; Zhang, C. One-Pot Synthesis of Diiron Phosphide/Nitrogen-Doped Graphene Nanocomposite for Effective Hydrogen Generation. *Nano Energy* **2015**, *12*, 666−674.
(46) Qian, C.; Kim, F.; Ma, L.; Tsui, F.; Yang, P.; Liu, J. Solution-Phase Synthesis of Single-Crystalline Iron Phosphide Nanorods/Nanowires. *J. Am. Chem. Soc.* **2004**, *126*, 1195−1198.
(47) Powell, C. Recommended Auger Parameters for 42 Elemental Solids. *J. Electron Spectrosc. Relat. Phenom.* **2012**, *185*, 1−3.
(48) Grosvenor, A. P.; Wik, S. D.; Cavell, R. G.; Mar, A. Examination of the Bonding in Binary Transition-Metal Monophosphides MP (M = Cr, Mn, Fe, Co) by X-Ray Photoelectron Spectroscopy. *Inorg. Chem.* **2005**, *44*, 8988−8998.
(49) Jiang, N.; You, B.; Sheng, M.; Sun, Y. Electrodeposited Cobalt-Phosphorous-Derived Films as Competent Bifunctional Catalysts for Overall Water Splitting. *Angew. Chem., Int. Ed.* **2015**, *54*, 6251−6254.
(50) Saadi, F. H.; Carim, A. I.; Verlage, E.; Hemminger, J. C.; Lewis, N. S.; Soriaga, M. P. CoP as an Acid-Stable Active Electrocatalyst for the Hydrogen-Evolution Reaction: Electrochemical Synthesis, Interfacial Characterization and Performance Evaluation. *J. Phys. Chem. C* **2014**, *118*, 29294−29300.
(51) Xiong, D.; Wang, X.; Li, W.; Liu, L. Facile Synthesis of Iron Phosphide Nanorods for Efficient and Durable Electrochemical Oxygen Evolution. *Chem. Commun.* **2016**, *52*, 8711−8714.
(52) Wang, P.; Song, F.; Amal, R.; Ng, Y. H.; Hu, X. Efficient Water Splitting Catalyzed by Cobalt Phosphide-Based Nanoneedle Arrays Supported on Carbon Cloth. *ChemSusChem* **2016**, *9*, 472−477.
(53) Jung, S.; McCrory, C. C.; Ferrer, I. M.; Peters, J. C.; Jaramillo, T. F. Benchmarking Nanoparticulate Metal Oxide Electrocatalysts for the Alkaline Water Oxidation Reaction. *J. Mater. Chem. A* **2016**, *4*, 3068−3076.
(54) McCrory, C. C.; Jung, S.; Ferrer, I. M.; Chatman, S. M.; Peters, J. C.; Jaramillo, T. F. Benchmarking Hydrogen Evolving Reaction and Oxygen Evolving Reaction Electrocatalysts for Solar Water Splitting Devices. *J. Am. Chem. Soc.* **2015**, *137*, 4347−4357.
(55) McCrory, C. C.; Jung, S.; Peters, J. C.; Jaramillo, T. F. Benchmarking Heterogeneous Electrocatalysts for the Oxygen Evolution Reaction. *J. Am. Chem. Soc.* **2013**, *135*, 16977−16987.
(56) Faber, M. S.; Dziedzic, R.; Lukowski, M. A.; Kaiser, N. S.; Ding, Q.; Jin, S. High-Performance Electrocatalysis Using Metallic Cobalt Pyrite (CoS_2) Micro-and Nanostructures. *J. Am. Chem. Soc.* **2014**, *136*, 10053−10061.
(57) Liu, M.; Li, J. Cobalt Phosphide Hollow Polyhedron as Efficient Bifunctional Electrocatalysts for the Evolution Reaction of Hydrogen and Oxygen. *ACS Appl. Mater. Interfaces* **2016**, *8*, 2158−2165.
(58) Jia, X.; Zhao, Y.; Chen, G.; Shang, L.; Shi, R.; Kang, X.; Waterhouse, G. I.; Wu, L. Z.; Tung, C. H.; Zhang, T. Ni_3FeN Nanoparticles Derived from Ultrathin NiFe-Layered Double Hydroxide Nanosheets: An Efficient Overall Water Splitting Electrocatalyst. *Adv. Energy Mater.* **2016**, *6*, 1502585.
(59) Xia, C.; Jiang, Q.; Zhao, C.; Hedhili, M. N.; Alshareef, H. N. Selenide-Based Electrocatalysts and Scaffolds for Water Oxidation Applications. *Adv. Mater.* **2016**, *28*, 77−85.
(60) Zhang, B.; Zheng, X.; Voznyy, O.; Comin, R.; Bajdich, M.; García-Melchor, M.; Han, L.; Xu, J.; Liu, M.; Zheng, L.; et al. Homogeneously Dispersed Multimetal Oxygen-Evolving Catalysts. *Science* **2016**, *352*, 333−337.
(61) Pi, Y.; Zhang, N.; Guo, S.; Guo, J.; Huang, X. Ultrathin Laminar Ir Superstructure as Highly Efficient Oxygen Evolution Electrocatalyst in Broad pH Range. *Nano Lett.* **2016**, *16*, 4424−4430.
(62) Fu, S.; Zhu, C.; Song, J.; Engelhard, M. H.; Li, X.; Du, D.; Lin, Y. Highly Ordered Mesoporous Bimetallic Phosphides as Efficient Oxygen Evolution Electrocatalysts. *ACS Energy Lett.* **2016**, *1*, 792−796.
(63) Zhan, Y.; Lu, M.; Yang, S.; Liu, Z.; Lee, J. Y. The Origin of Catalytic Activity of Nickel Phosphate for Oxygen Evolution in Alkaline Solution and Its Further Enhancement by Iron Substitution. *ChemElectroChem* **2016**, *3*, 615−621.
(64) Xu, X.; Song, F.; Hu, X. A Nickel Iron Diselenide-Derived Efficient Oxygen-Evolution Catalyst. *Nat. Commun.* **2016**, *7*, 12324.
(65) Chen, J. Y.; Dang, L.; Liang, H.; Bi, W.; Gerken, J. B.; Jin, S.; Alp, E. E.; Stahl, S. S. Operando Analysis of NiFe and Fe Oxyhydroxide Electrocatalysts for Water Oxidation: Detection of Fe^{4+} by MöSsbauer Spectroscopy. *J. Am. Chem. Soc.* **2015**, *137*, 15090−15093.
(66) Deng, J.-F.; Li, H.; Wang, W. Progress in Design of New Amorphous Alloy Catalysts. *Catal. Today* **1999**, *51*, 113−125.
(67) Imanishi, A.; Okamura, T.; Ohashi, N.; Nakamura, R.; Nakato, Y. Mechanism of Water Photooxidation Reaction at Atomically Flat TiO_2 (Rutile) (110) and (100) Surfaces: Dependence on Solution pH. *J. Am. Chem. Soc.* **2007**, *129*, 11569−11578.

DOI: 10.1021/acsenergylett.7b00206
ACS Energy Lett. 2017, 2, 1035−1042